

An Analysis of ISAR Image Distortion Based on the Phase Modulation Effect

S. K. Wong, E. Riseborough, and G. Duff

Defence R&D Canada - Ottawa, 3701 Carling Avenue, Ottawa, ON, Canada K1A 0Z4

Received 28 April 2005; Revised 26 August 2005; Accepted 16 December 2005

Distortion in the ISAR image of a target is a result of nonuniform rotational motion of the target during the imaging period. In many of the measured ISAR images from moving targets, such as those from in-flight aircraft, the distortion can be quite severe. Often, the image integration time is only a few seconds in duration and the target's rotational displacement is only a few degrees. The conventional quadratic phase distortion effect is not adequate in explaining the severe blurring in many of these observations. A numerical model based on a time-varying target rotation rate has been developed to quantify the distortion in the ISAR image. It has successfully modelled the severe distortion observed; the model's simulated results are validated by experimental data. Results from the analysis indicate that the severe distortion is attributed to the phase modulation effect where a time-varying Doppler frequency provides the smearing mechanism. For target identification applications, an efficient method on refocusing distorted ISAR images based on time-frequency analysis has also been developed based on the insights obtained from the results of the numerical modelling and experimental investigation conducted in this study.

Copyright © 2006 Hindawi Publishing Corporation. All rights reserved.

1. INTRODUCTION

Inverse synthetic aperture radar (ISAR) imaging provides a 2-dimensional radar image of a target. A 2-dimensional picture can potentially offer crucial information about the features of the target and provide improved discrimination, leading to more accurate target identification. An ISAR image of a target is generated as a result of the target's rotational motion. This motion can sometimes be quite complex, such as that of a fast, manoeuvring jet aircraft. As a result, severe distortion can occur in the ISAR image of the target [1]. An illustration of a distorted ISAR image of an aircraft is shown in Figure 1(a); it can be seen clearly that the ISAR image is severely blurred. It has been recognized that a time-varying rotating motion from the rotation of the target is responsible for the image blurring [2]. Figure 2(a) shows the azimuth angular displacements of the aircraft in Figure 1(a) as a function of time, as recorded independently by a ground-truth instrument mounted on-board the aircraft. When the target's rotation is relatively smooth (Figure 2(b)), the measured ISAR image of the aircraft is relatively well focused; this is illustrated in Figure 1(b). In addition, the temporal phase histories of a scattering centre on the aircraft from both the blurred and focused ISAR images also display the same temporal behaviour as the rotating azimuth motion of the aircraft; this is illustrated in Figures 2(c) and 2(d), respectively.

It is clearly seen that there is a direct correspondence between the distortion in the ISAR image and the nonuniform rotational motion of the target.

Although the distortion in ISAR images has been recognized as due to the higher-order Doppler motion effect from the target's rotation [3], much of the analysis on ISAR distortion is focused on the second-order effect of the target's rotational motion [2, 3] and the distortion is conventionally attributed to the quadratic phase effect [4, 5]. This quadratic phase error is a result of a constant circular motion of the target with respect to the radar, resulting in a nonconstant Doppler velocity introduced along the radar's line of sight due to the acceleration of the target from the circular motion [4]. Quadratic phase distortion is significant only when the target image is integrated over a large angular rotation by the target and it does not provide an adequate account of the severe blurring in many of the observed ISAR images from real targets. Furthermore, time-frequency analysis of the distorted ISAR images often reveals that the motion of the target is fluctuating randomly and displays no temporal quadratic phase behaviour.

In order to obtain a better understanding of the severe distortion in ISAR images, we have developed a numerical model that is based on a time-varying target rotational motion to simulate the observed distortion. It will be shown that this model provides an accurate representation of the

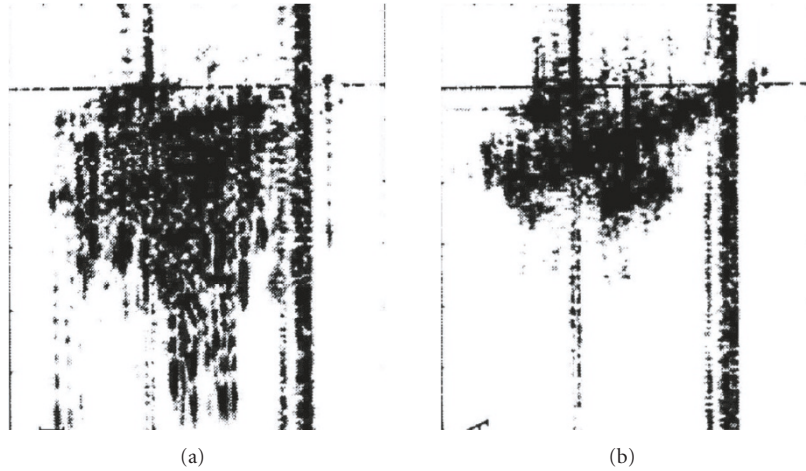


FIGURE 1: Example of (a) a distorted ISAR image and (b) an undistorted ISAR image of an in-flight aircraft [1].

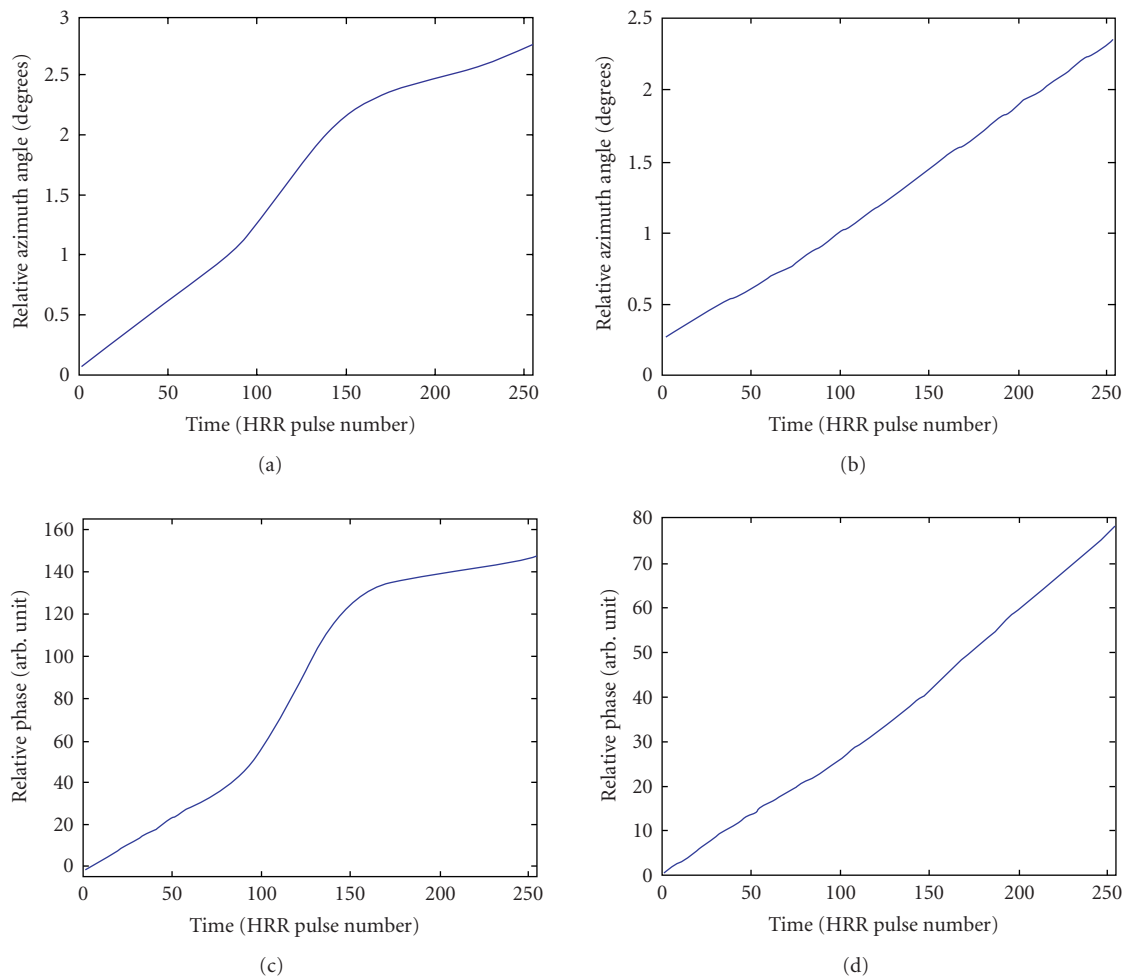


FIGURE 2: The azimuth angular displacements of the aircraft in Figure 1 during the ISAR imaging period for the (a) distorted ISAR image in Figure 1(a), (b) focused ISAR image in Figure 1(b). The temporal phase history of a scattering centre on the aircraft for the (c) distorted ISAR image (Figure 1(a)), (d) focused ISAR image (Figure 1(b)). The imaging period is 4.6 seconds, corresponding to a sequence of 256 HRR profiles in composing the ISAR images.

distorting mechanism. This model includes many higher-order terms in the Doppler motion beyond the quadratic term in the phase of the target echo that some of the current analysis employed [2–6]. Experiments are conducted to study and to demonstrate the severe distortion in ISAR images. The measured data are used for comparing and validating the model’s simulated results. The comparative results indicate that the model provides an accurate account of the ISAR distortion. The distortion can be attributed to a modulation effect in the phase of the target echo as a result of a time-varying Doppler motion of the target. It will also be shown that the quadratic phase distortion may be seen as a special case of the phase modulation effect; however, it cannot account for the severe distortion as observed in measured data.

For target recognition applications, a blurred ISAR image has to be refocused so that it can be used for target identification. Time-frequency signal processing techniques can be applied to effectively refocus distorted ISAR images [6]. In time-frequency processing, an ISAR image of a target is extracted from a short-time interval; a focused image is thus obtained because the target’s motion can be considered as relatively uniform over a short duration. However, there are a large number of subintervals to deal with in the refocusing processing. It is very time-consuming to examine all refocused ISAR images to search for the best image. An efficient ISAR refocusing procedure is developed to extract an optimum refocused image quickly without having to process a large number of images systematically. Issues such as how to locate the appropriate time instant to extract the best refocused image [7] and how to determine the appropriate time window width [8] will also be discussed.

2. ISAR IMAGING OF A MOVING TARGET

In general, a moving target could possess pitch, roll, and yaw motions simultaneously, in addition to a translational motion at any given instant of time. These motions all contribute to a resultant rotation of the target with respect to the radar that defines the formation of an ISAR image of the target. For a target with an arbitrary orientation relative to the radar, the various motions of the target are depicted in Figure 3. The phase in the radar echo of a scatterer on the target is given by

$$\phi = \frac{4\pi f}{c} R(t), \quad (1)$$

where $R(t)$ is the line-of-sight distance between the scatterer and the radar. Since the radar can detect a target’s motion along the radar’s line of sight only, it is therefore logical to define a target coordinate reference system in which the x -axis is parallel to the radar’s line of sight; this is illustrated in Figure 3. The changes in $R(t)$ during the imaging interval can be expressed in terms of the target’s motion parameters as

$$R(t) = R_0 - \int_0^t (\mathbf{v}(\tau) \cdot \mathbf{x}) d\tau - \int_0^t (\boldsymbol{\omega}(\tau) \times \mathbf{r}(\tau)) \cdot \mathbf{x} d\tau, \quad (2)$$

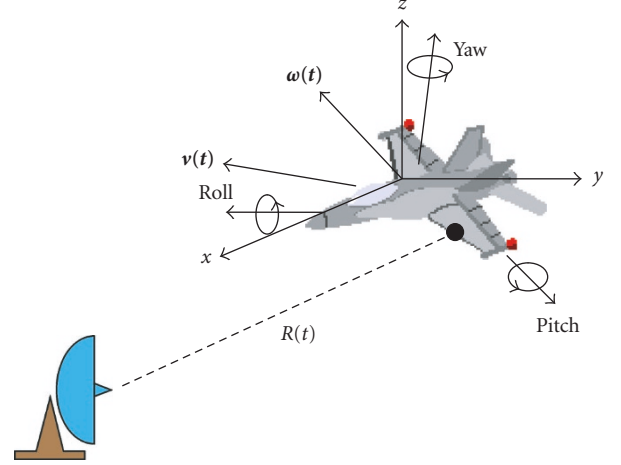


FIGURE 3: Various motions possessed by a moving target.

where R_0 is the initial distance between the scatterer and the radar at the beginning of the imaging scan. The second term is the radial displacement of the scatterer due to the translational motion of the target; \mathbf{v} is the translational velocity vector and \mathbf{x} denotes the unit directional vector parallel to the radar’s line of sight. The third term is the line-of-sight displacement of the scatterer as a result of the rotational motion of the target; $\boldsymbol{\omega}$ is the rotational vector from the resultant angular motion of the target and \mathbf{r} is the positional vector of the scatterer on the target measured from the intersection of $\boldsymbol{\omega}$ and the x -axis (see Figure 4). The rotational motion of the target provides a Doppler frequency shift that allows the scatterer to be imaged along the cross-range of the ISAR image. The Doppler frequency at time t is given by

$$f_D = \frac{4\pi f}{c} ((\boldsymbol{\omega}(t) \times \mathbf{r}(t)) \cdot \mathbf{x}), \quad (3)$$

where f is the radar frequency. The resultant rotational vector $\boldsymbol{\omega}$ includes the pitch, roll, and yaw motions, as well as any relative rotation as a result of the translational motion of the target relative to the radar. As an example, an aircraft flying across in front of the radar from one side to the other will produce an apparent yaw motion of the target as seen by the radar tracking the movement of the aircraft. The rotational displacement of a scatterer on the target

$$\mathbf{X}(t) = \int_0^t (\boldsymbol{\omega}(\tau) \times \mathbf{r}(\tau)) d\tau \quad (4)$$

provides the Doppler motion information on the phase of the radar echo for the ISAR image processing.

Instead of solving (4) by applying the methods of classical rigid-body mechanics, a more physical approach is taken. The displacement of a scatterer due to rotation in (4) can be

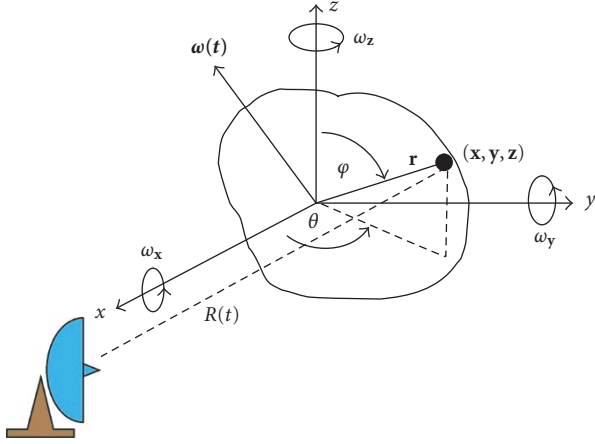


FIGURE 4: A Cartesian coordinate reference frame for the target with respect to the radar. The x -axis is aligned parallel to the radar's line of sight.

rewritten as

$$\begin{aligned} \mathbf{X}(t) &= \int_0^t (\boldsymbol{\omega}(\tau) \times \mathbf{r}(\tau)) d\tau = \int_0^t \mathbf{v}_R(\tau) d\tau = \int_0^t \frac{d\mathbf{x}_R(\tau)}{d\tau} d\tau \\ &= \int_{\mathbf{x}_0}^{\mathbf{x}_t} d\mathbf{x}_R = (x(t) - x_0)\mathbf{x} + (y(t) - y_0)\mathbf{y} + (z(t) - z_0)\mathbf{z} \end{aligned} \quad (5)$$

for a general arbitrary rotation in which a scatterer on the target moves from coordinates (x_0, y_0, z_0) at $t_0 = 0$ to a new position at (x, y, z) at time t during a small time interval $\Delta t = t - t_0$ and $\mathbf{x}, \mathbf{y}, \mathbf{z}$ are the unit directional vectors. Moreover,

the rotational vector $\boldsymbol{\omega}$ of the target can be decomposed into three orthogonal components; that is,

$$\boldsymbol{\omega}(t) = \omega_x(t)\mathbf{x} + \omega_y(t)\mathbf{y} + \omega_z(t)\mathbf{z}. \quad (6)$$

This is shown in Figure 4, and $\omega_x(t)$, $\omega_y(t)$, and $\omega_z(t)$ are the amplitudes of the three orthogonal rotating components (rad/s). It is intuitively obvious from Figure 4 that only the rotational components rotating about the z -axis ($\omega_z\mathbf{z}$) and rotating about the y -axis ($\omega_y\mathbf{y}$) of the target will have contribution to the displacement along the x -axis (i.e., along the radar's line of sight). The change in the position of the scatterer as a result of a rotation about the z -axis is given by

$$\begin{pmatrix} x \\ y \\ z \end{pmatrix} = \begin{pmatrix} \cos(\Delta\theta) & -\sin(\Delta\theta) & 0 \\ \sin(\Delta\theta) & \cos(\Delta\theta) & 0 \\ 0 & 0 & 1 \end{pmatrix} \begin{pmatrix} x_0 \\ y_0 \\ z_0 \end{pmatrix}, \quad (7)$$

where $\Delta\theta = \omega_z\Delta t$ is the amount of rotation parallel to the x - y plane. This is the rotational motion that causes a change in the azimuth of the target as seen from the radar's perspective. The change in the position of the scatterer rotating about the y -axis is given by

$$\begin{pmatrix} x \\ y \\ z \end{pmatrix} = \begin{pmatrix} \cos(\Delta\varphi) & 0 & \sin(\Delta\varphi) \\ 0 & 1 & 0 \\ -\sin(\Delta\varphi) & 0 & \cos(\Delta\varphi) \end{pmatrix} \begin{pmatrix} x_0 \\ y_0 \\ z_0 \end{pmatrix}, \quad (8)$$

where $\Delta\varphi = \omega_y\Delta t$ is the amount of rotation about the y -axis. This is the rotational motion that causes a change in the elevation of the target as seen by the radar. The combined resultant displacement can be expressed as

$$\begin{aligned} \begin{pmatrix} x \\ y \\ z \end{pmatrix} &= \begin{pmatrix} \cos(\Delta\varphi) & 0 & \sin(\Delta\varphi) \\ 0 & 1 & 0 \\ -\sin(\Delta\varphi) & 0 & \cos(\Delta\varphi) \end{pmatrix} \begin{pmatrix} \cos(\Delta\theta) & -\sin(\Delta\theta) & 0 \\ \sin(\Delta\theta) & \cos(\Delta\theta) & 0 \\ 0 & 0 & 1 \end{pmatrix} \begin{pmatrix} x_0 \\ y_0 \\ z_0 \end{pmatrix} \\ &= \begin{pmatrix} \cos(\Delta\theta)\cos(\Delta\varphi) & -\sin(\Delta\theta)\cos(\Delta\varphi) & \sin(\Delta\varphi) \\ \sin(\Delta\theta) & \cos(\Delta\theta) & 0 \\ -\cos(\Delta\theta)\sin(\Delta\varphi) & \sin(\Delta\theta)\sin(\Delta\varphi) & \cos(\Delta\varphi) \end{pmatrix} \begin{pmatrix} x_0 \\ y_0 \\ z_0 \end{pmatrix}. \end{aligned} \quad (9)$$

Hence, the displacement of a scatterer along the x -axis is given by

$$\begin{aligned} X = x - x_0 &= [x_0(\cos(\Delta\theta)\cos(\Delta\varphi)) \\ &\quad - y_0(\sin(\Delta\theta)\cos(\Delta\varphi)) + z_0\sin(\Delta\varphi)] - x_0. \end{aligned} \quad (10)$$

This is a somewhat complex expression to keep track of in a numerical analysis and too complex to be used in a con-

trolled experiment. It would be much simpler to work with a rotation vector $\boldsymbol{\omega}$ that is parallel to the z -axis, for example, a yaw motion of the target as seen by the radar in Figure 4. Then, the general displacement of a scatterer given by (9) can be simplified to (7). Moreover, note that in (7), a 3-dimensional target rotating about the z -axis is reduced to a 2-dimensional problem; that is, the z coordinate of a scatterer on the target does not change in a rotation about the z -axis. Thus one can further simplify the problem by considering a

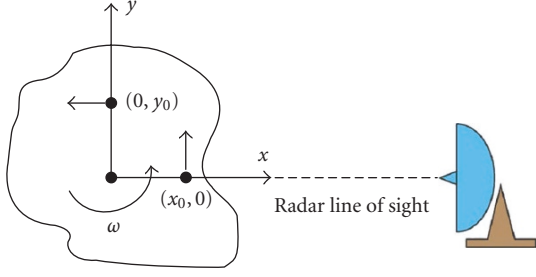


FIGURE 5: Schematic of a rotating target with examples of two scattering centres illustrated. The target is rotating about the z -axis (out of page).

2-dimensional target with scatterers located on the x - y plane parallel to the line of sight, rotating about the z -axis; this is illustrated in Figure 5. It should be emphasized that the simplification of the target geometry does not alter the physics of the problem; rather, it offers a clearer physical insight of the problem by removing the unnecessary clutters in the algebra.

3. ISAR DISTORTION MODEL

In order to bring out the basic ISAR distortion mechanism more clearly, we will consider just one scatterer on the target in the following analysis. This allows us to illustrate the physics analytically without any loss of generality. From (1) and (2), the phase of the radar return signal from a scatterer on a moving target is given by

$$\phi = \frac{4\pi f}{c} (R_0 - vt - X(t)), \quad (11)$$

where f is the transmitting radar frequency, R_0 is the initial distance of the scatterer on the target from the radar at the onset of the radar imaging scan, v is the radial velocity of the scatterer, and $X(t)$ is the displacement due to the rotation of the scatterer along the radar's line of sight. Using the target geometry as shown in Figure 5, a change in the scatterer's coordinates due to a rotation about the z -axis at a later time t can be expressed succinctly as

$$\begin{pmatrix} x(t) \\ y(t) \end{pmatrix} = \begin{pmatrix} \cos(\omega(t)t) & -\sin(\omega(t)t) \\ \sin(\omega(t)t) & \cos(\omega(t)t) \end{pmatrix} \begin{pmatrix} x_0 \\ y_0 \end{pmatrix} \quad (12)$$

according to (7). The displacement along the radar's line of sight $X(t) = x(t) - x_0$ due to a rotation of the target is then given by

$$X(t) = (x_0 \cos(\omega(t)t) - y_0 \sin(\omega(t)t)) - x_0. \quad (13)$$

Thus an $X(t)$ due to a time-varying rotational motion during the ISAR imaging period can be modelled by a series of small displacements using (13) to cover the whole imaging duration. Note that the rotational rate in (13) is expressed as a function of time; that is, $\omega(t)$. A time-varying rotational rate can be fitted, in general, by a Fourier series; that is,

$$\omega(t) \approx \omega_0 + \sum_{n=1}^{\infty} \left(a_n \cos\left(\frac{n\pi t}{T}\right) + b_n \sin\left(\frac{n\pi t}{T}\right) \right), \quad (14)$$

where ω_0 is the constant rotational rate of the target in the absence of any extraneous fluctuation in the rotational motion, T is the ISAR imaging period and a_n, b_n can be considered as random variables for fitting $\omega(t)$ to any fluctuating motion during the imaging period, $0 \leq t \leq T$. Note that it is customary to use the symbol \approx in the Fourier series equation (14) to indicate that the series on the right-hand side may not necessarily converge exactly to $\omega(t)$.

An ISAR image is generated using a sequence of high range resolution (HRR) profiles. Firstly, detected target echoes are demodulated and converted into digitized in-phase and quadrature (I, Q) signals in the frequency domain. Then, the HRR profile of a scatterer can be generated by applying a discrete Fourier transform to the frequency-domain in-phase and quadrature signal data [9],

$$\begin{aligned} H_n &= \sum_{i=0}^{N-1} (I + jQ)_i \exp\left(j\frac{2\pi}{N}ni\right) \\ &= h_n \exp\left(j\frac{4\pi f_c}{c}(R_0 - vt - X(t))\right) \exp\left(j\frac{N-1}{N}\pi n\right), \end{aligned} \quad (15)$$

where h_n is the amplitude of the HRR profile with a $\sin(Nx)/\sin(x)$ envelop, n is the range-bin index, $n = 0, \dots, N-1$; f_c is the centre frequency of the radar bandwidth, and R_0 and $X(t)$ are defined in (11). A second discrete Fourier transform is then performed at each of the range bins over the sequence of HRR profiles to generate an ISAR image; that is,

$$\begin{aligned} I_{n,m} &= \sum_{k=0}^{M-1} h_{n,k} \exp\left(j\frac{4\pi f_c}{c}(R_0 - vt - X(t))\right) \\ &\quad \times \exp\left(j\frac{N-1}{N}\pi n\right) \exp\left(j\frac{2\pi}{M}mk\right), \end{aligned} \quad (16)$$

where m is the cross-range bin index, $m = 0, \dots, M-1$. M is the number of HRR profiles used in the generation of the ISAR image. The radial target motion is assumed to be compensated; that is, vt is set to zero. In effect, the second Fourier transform converts the HRR variable at each range bin from the time domain into the frequency domain. Hence, the cross-range dimension of the ISAR image represents the Doppler frequency as observed by the radar. The term that is of interest in the analysis of the distortion in an ISAR image is the phase factor containing the temporal rotational displacement $X(t)$ in (16); that is,

$$\begin{aligned} \psi(t) &= \exp\left[-j\frac{4\pi f_c}{c}X(t)\right] \\ &= \exp\left[-j\frac{4\pi f_c}{c}((x_0 \cos(\omega(t)t) - y_0 \sin(\omega(t)t)) - x_0)\right]. \end{aligned} \quad (17)$$

Equation (17) forms the basis of the numerical model for computing the ISAR distortion of a target due to a time-varying rotational motion.

It would also be instructive to show that the ISAR distortion effect is a result of a time-dependent rotational motion

analytically. This would give us a better physical insight of the problem. To derive an analytical expression for the distortion mechanism, the phase factor due to rotation is rewritten as

$$\begin{aligned}\psi(t) &= \exp\left(-j\frac{4\pi f_c}{c}X(t)\right) \\ &= \exp\left(-j\frac{4\pi f_c}{c}\int_0^t (\boldsymbol{\omega}(\tau) \times \mathbf{r}(\tau)) \cdot \mathbf{x}d\tau\right) \quad (18) \\ &= \exp\left(-j\frac{4\pi f_c}{c}\int_0^t \|\boldsymbol{\omega}(\tau)\| \|\mathbf{r}(\tau)\| \sin\theta d\tau\right)\end{aligned}$$

by substituting (4) for $X(t)$. Then, consider a short-time instant when the scatterer is located at $(0, y_0)$ where the scatterer's motion is parallel to the radar's line of sight (see Figure 5); this corresponds to the largest Doppler effect as seen by the radar. To obtain an analytical expression, two simplifying steps are taken. First, a simplified time-varying rotational rate is assumed and is given by

$$\boldsymbol{\omega}(t) = \boldsymbol{\omega}_0 + \boldsymbol{\omega}_r \sin(2\pi\Omega t), \quad (19)$$

where $\boldsymbol{\omega}_0$ is a constant, $\boldsymbol{\omega}_r$ is the rotational amplitude of the fluctuating motion, and Ω is the fluctuating frequency of the time-varying motion. A second simplifying step is to assume that the distance between the scatterer at $(0, y_0)$ and the rotation centre of the target is more or less constant such that $\|\mathbf{r}(t)\| \approx y_0$ during this time instant as depicted in Figure 5. This assumption is a reasonable one because normally, the ISAR image of a target is captured during a relatively small rotation of the target. For example, the ISAR images generated in Figure 1 correspond to a rotation of only about 3 degrees; hence $\|\mathbf{r}(t)\|$ is nearly constant. Furthermore, $\sin\theta$ is set to -1 (in (18)), corresponding to $\theta = -90$ degrees as measured from the x -axis in Figure 5; this is consistent with the target geometry shown in Figure 5 where the scatterer at $(0, y_0)$ has the maximum Doppler velocity and is moving away from the radar. Applying these 2 simplifying assumptions and substituting (19) into (18),

$$\begin{aligned}\psi(t) &= \exp\left[j\frac{4\pi f_c}{c}y_0\int_0^t \|\boldsymbol{\omega}(\tau)\|d\tau\right] \\ &= \exp\left[j\frac{4\pi f_c}{c}y_0\int_0^t (\boldsymbol{\omega}_0 + \boldsymbol{\omega}_r \sin(2\pi\Omega\tau))d\tau\right] \\ &= \exp\left[j\frac{4\pi f_c}{c}y_0\boldsymbol{\omega}_0 t\right] \exp\left[j\frac{4\pi f_c}{c}y_0\boldsymbol{\omega}_r\int_0^t \sin(2\pi\Omega\tau)d\tau\right]. \quad (20)\end{aligned}$$

The first factor in (20) corresponds to a constant rotation of the target. This factor provides a Doppler shift that allows the scatterer to be imaged along the cross-range dimension to form an undistorted ISAR image of the target in the absence of any fluctuating motion. The second factor describes a phase modulation effect due to a temporally fluctuating motion of the scatterer that introduces distortion in the ISAR image. To see how the phase modulation effect comes about more clearly, the second phase factor in (20) can be rewritten

as

$$\begin{aligned}\mu(t) &= \exp\left[j\frac{4\pi f_c}{c}y_0\boldsymbol{\omega}_r\int_0^t \sin(2\pi\Omega\tau)d\tau\right] \\ &= \exp(jk \sin(\eta)) \\ &= \cos(k \sin(\eta)) + j \sin(k \sin(\eta)) \\ &= (J_0(k) + 2J_2(k) \cos(2\eta) + 2J_4(k) \cos(4\eta) + \dots) \\ &\quad + j(2J_1(k) \sin(\eta) + 2J_3(k) \sin(3\eta) \\ &\quad + 2J_5(k) \sin(5\eta) + \dots), \quad (21)\end{aligned}$$

where

$$\begin{aligned}k &= \frac{4\pi f_c}{c}y_0, \\ \eta &= \sin^{-1}\left[\boldsymbol{\omega}_r\int_0^t \sin(2\pi\Omega\tau)d\tau\right], \quad (22)\end{aligned}$$

and the J_n are the Bessel functions of the first kind of order n . It can be seen from (21) that the phase of a time-dependent rotational motion consists of many higher-order sideband components. These higher-order sideband components are a consequence of phase modulation from a temporally fluctuating target motion and they have been shown to produce a smear in the radar image as a result [10].

4. ISAR DISTORTION EXPERIMENTS

An ISAR experiment is set up to examine the distortion in ISAR images due to a time-varying rotational motion. There are a number of reasons why data from a controlled experiment are desirable. In a controlled experiment, the locations of the scattering centres and the rotational axis of the target are known precisely. The rotational motion of the target can be programmed and controlled to produce the desired effects that are sought for analysis. Moreover, experiments of a given set of conditions can be repeated to verify the consistency of the results. These are not always possible with real targets such as in-flight aircraft. Data from controlled experiments can then be used to compare with simulated results from the numerical model under the same set of conditions. Such comparison provides a meaningful validation of the numerical model, thus providing a clearer picture of the distorting process.

A 2-dimensional delta wing shaped target, the target motion simulator (TMS), is built for the ISAR distortion experiments. A picture of the TMS is shown in Figure 6. The target has a length of 5 m on each of its three sides. Six trihedral reflectors are mounted on the TMS as scattering centres of the target; all the scatterers are located on the x - y plane. They are designed to always face towards the radar as the TMS rotates. The TMS target is set up so that it is rotating perpendicular to the radar line of sight. This simplified target geometry is identical to the one used in the numerical model given in the previous section. Hence, the experimental data from the TMS target can be used to compare with the model's simulated results. Figure 7 shows a schematic of the



FIGURE 6: The target motion simulator (TMS) experimental apparatus.

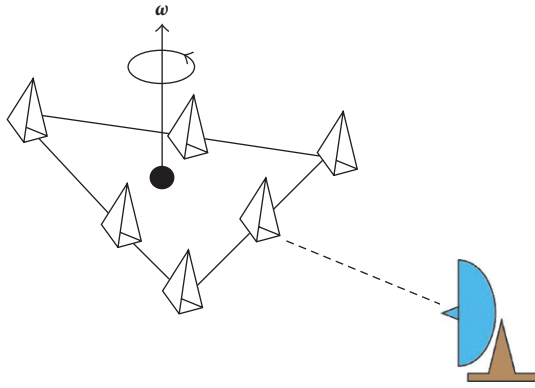


FIGURE 7: Schematic of the ISAR imaging experimental setup.

experimental setup; note that one corner reflector is placed asymmetrically to provide a relative geometric reference of the TMS target. A time-varying rotational motion is introduced by a programmable motor drive. ISAR images of the TMS target are collected at X-band from 8.9 GHz to 9.4 GHz using a stepped frequency radar waveform with a frequency step size of 10 MHz and a radar repetition rate PRF = 2 kHz. A sequence of ISAR images of the TMS apparatus is shown in Figure 8, corresponding to the target making a transition from a constant rotation (Figure 8(a)) to a time-varying rotational motion (Figures 8(b) and 8(c)). Figure 8(a) shows an ISAR image that is well focused with the 6 reflectors shown clearly; the target is rotating with a constant motion of about 2.0 degrees/s. A fluctuating motion is then added to the motion of the target. The ISAR images become distorted as seen in Figures 8(b) and 8(c). The actual fluctuating target motion that corresponds to the distortion in Figure 8(c) is shown in Figure 9(a); the motion is extracted from the experimental ISAR image as a time-frequency spectrogram [9]. The rotational displacement of the target is shown in Figure 9(b). The target has rotated 8 degrees during a 4-second imaging interval. The fluctuating motion is clearly evident from the rippling behaviour of the rotational displacement of the target in Figure 9(b). It is also evident that the fluctuating rotational motion deviates less than 1 degree from a smooth uniform rotating motion (dashed line in Figure 9(b)) at any given instant of time during the imaging interval. This serves to

illustrate that even though the amount of perturbed motion on the target is very small, the amount of distortion introduced in the ISAR image of the target can be quite significant as shown in Figure 8(c). This result is consistent with the severe distortion observed from a real target as shown in Figure 1(a).

5. ISAR DISTORTION ANALYSIS

A distorted ISAR image of the TMS target computed by the numerical model based on (17) is shown in Figure 10; the computation is done using the experimental parameters as inputs. It can be seen from Figure 10 that the computed distortion in the ISAR image compares quite well with the experimental image as shown in Figure 8(c). Figure 11 shows another comparison of a distorted ISAR image of the TMS target between experiment and computation from another imaging experiment using an FM-modulated pulse compression radar waveform with a 300 MHz bandwidth at 10 GHz [9]. It can also be seen that there is again good agreement between the measured image and the computed image. Detailed analysis of the distortion displayed in the ISAR images has attributed the distortion as a consequence of the phase modulation effect in which a time-varying Doppler motion causes the image of the scatterer to smear along the cross-range axis of the ISAR image [9].

Analytically, the distortion due to phase modulation can be described in terms of a series of higher-order excitation described by the Bessel functions as given in (21). However, it would be more insightful and easier to understand the phase modulation effect by giving a more physical description. Using the temporal motion shown in Figure 9(a) as input, the Doppler frequency for scatterer #1 on the TMS target (see Figure 8(d)) is extracted from the numerical model as a time-frequency spectrogram [9]; this is shown in Figure 12(a). The corresponding distorted ISAR image of scatterer #1 is shown in Figure 12(b). It can be seen that the amount of distortion produced on scatterer #1 in the cross-range is the same as the amount of change in the Doppler frequency ($f_{D,\max} - f_{D,\min}$) possessed by scatterer #1 during the imaging interval. This result is expected since the cross-range dimension of the ISAR image is actually the Doppler frequency as explained in Section 3. Note that scatterer #6 in the ISAR image of Figure 12(b) has hardly any distortion. It corresponds to a scatterer located at $(x_0, 0)$ in Figure 5. The Doppler frequency of scatterer #6 is shown in Figure 13(a). It is essentially constant over the imaging duration; hence there is no noticeable distortion induced in the ISAR image. The phase factor for a small-angle rotation, according to (17), can be approximated by

$$\psi(t) = \exp \left[-j \frac{4\pi f_c}{c} \left(x_0 \frac{(\omega(t)t)^2}{2} - y_0 \omega(t)t \right) \right]. \quad (23)$$

The phase of scatterer #6 at $(x_0, 0)$ has only a second-order rotational effect; that is, $(\omega(t)t)^2$. This second-order term has a negligible distorting effect as seen in the computed image in Figure 12(b). By contrast, the distortion that occurs in scatterer #1 in Figure 12(b) is due to a very prominent

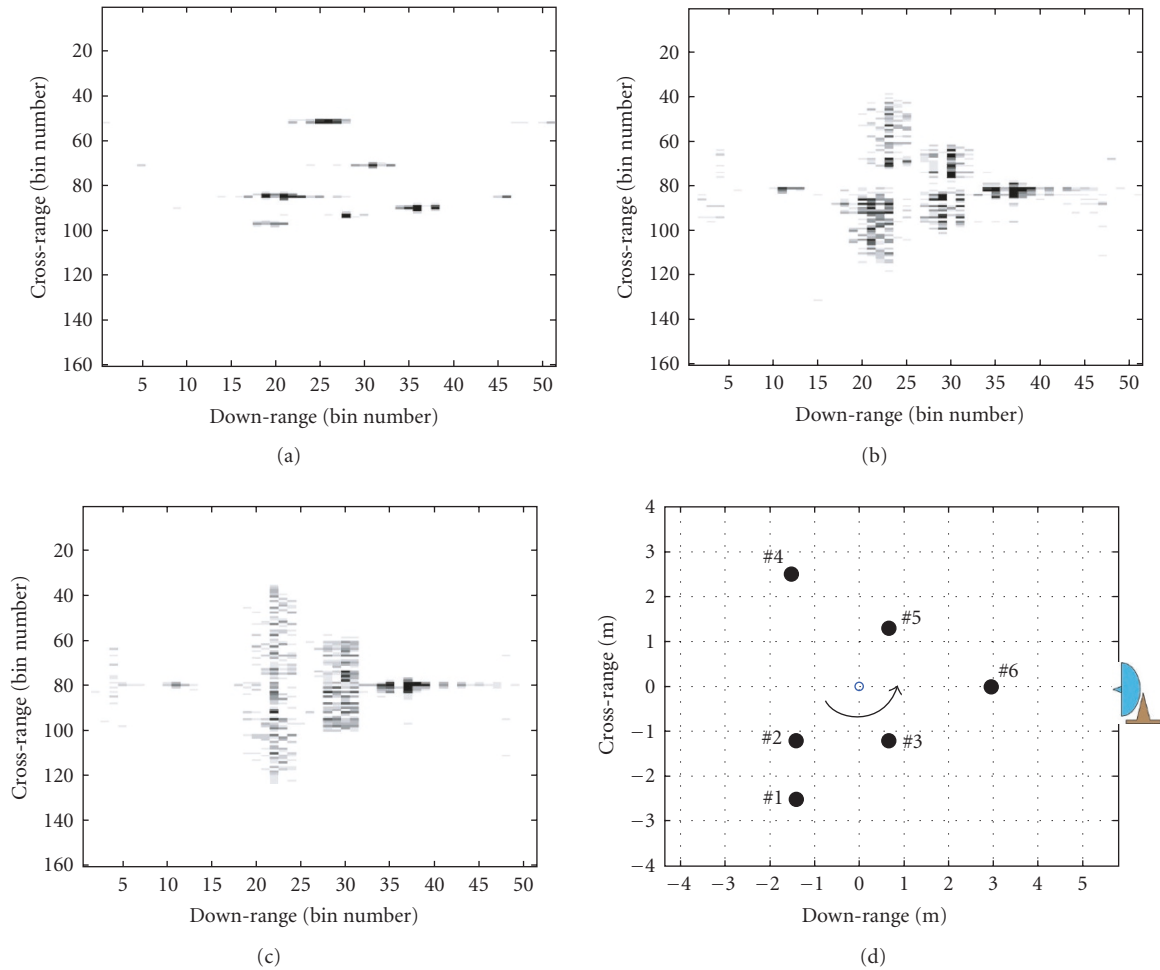


FIGURE 8: A sequence of measured ISAR images of the TMS target. (a) constant rotation at 2 degrees/s, (b) oscillating motion introduced to the target's rotating motion, (c) target with oscillating motion at a later time, and (d) the TMS target's orientation with respect to the radar for ISAR image in (c). The target is rotated in the counter-clockwise direction.

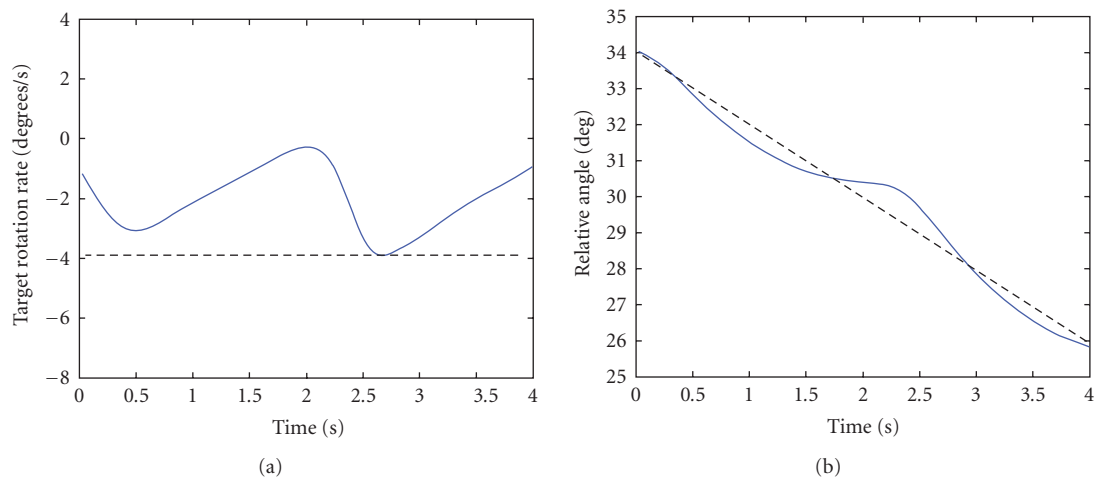


FIGURE 9: (a) Measured temporal motion (solid line) of the target motion simulator, (b) corresponding temporal rotational displacement (solid line) of target motion simulator. The dashed line indicates a constant rotational motion of the target.

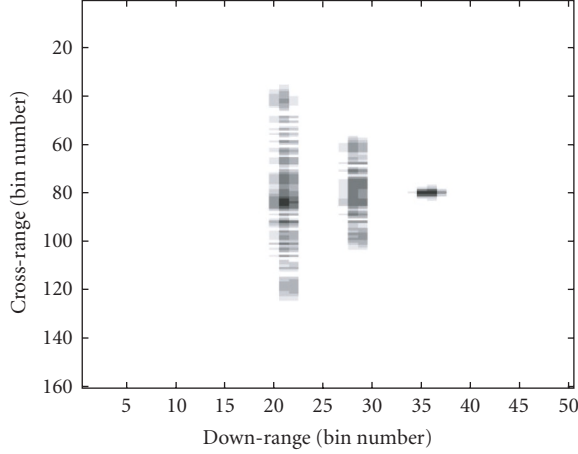


FIGURE 10: Computed distortion in the ISAR image using the phase modulation model. See and compare with the experimental image in Figure 8(c).

first-order component $\omega(t)t$ in (23). It should be stressed that even though the displacement $X(t)$ in a small-angle rotation is approximated up to the second order of the Taylor series for the sinusoids of (17), the time-varying rotational rate $\omega(t)$ in (23) is still given by a sinusoidal function. The sinusoidal function that describes $\omega(t)$ as given by (14) and (19) can be alternatively expressed using the Taylor series, for example,

$$\begin{aligned}\sin x &= x - \frac{x^3}{3!} + \frac{x^5}{5!} - \frac{x^7}{7!} + \dots \\ \cos x &= 1 - \frac{x^2}{2!} + \frac{x^4}{4!} - \frac{x^6}{6!} + \dots\end{aligned}\quad (24)$$

Hence, the time-varying motion of the target described in the present model is consistent with analyses presented in the literature in which the motion is expressed as a Taylor series [3, 5]. By expressing the time-varying rotation $\omega(t)$ using the sinusoidal functions, all the higher-order terms in the Taylor series are included implicitly in our model analysis. It is obvious that truncating the Taylor series to the first couple of terms will grossly misrepresent the temporally fluctuating motion and hence the ISAR distortion will not be fully accounted for by the lower-order approximation. The truncation of the Taylor series is valid only in the limiting case where the fluctuation in the time-varying motion of the target is not very significant during the imaging period; but this corresponds to a target that has largely a uniform rotational motion, and therefore there is little distortion expected in the ISAR image. We can thus summarize briefly by stating that a changing Doppler frequency of the scatterer due to the target's time-varying motion expressed through the variable $\omega(t)$ provides the physical basis for the large distortion in the ISAR image.

Another way of seeing the physical interpretation of the phase modulation effect can be illustrated using the experimental ISAR image shown in Figure 14(a). This distorted ISAR image provides a convenient illustration since there

exists a down-range bin where there is only one scatterer. The temporal behaviour of the Doppler frequency of this scatterer extracted using a time-frequency spectrogram is shown in Figure 14(c). Essentially, the spectrogram unfolds the distortion of scatterer #1 in the ISAR image (Figure 14(a)) as a function of time, providing a glimpse of the temporal change in the Doppler frequency during the ISAR imaging duration. In addition, phase information on scatterer #1 is also available from the image data; this is shown in Figure 14(b). It can be clearly seen that the phase is perturbed; that is, not a smooth function in time. By taking the time derivative of the phase, the instantaneous frequency (i.e., $1/2\pi(d\phi/dt)$) is obtained; this is shown in Figure 14(d). By comparing the Doppler frequency spectrogram in Figure 14(c) and the instantaneous frequency in Figure 14(d), it is quite evident that we have arrived at the same temporal history of the Doppler frequency for scatterer #1 via two different directions. From these two graphs, we can make a physical linkage, connecting the distortion introduced in the ISAR image to a time modulation effect in the phase of the scatterer. This illustration provides another perspective on the phase modulation effect. This effect has been validated by experimental data. Examples of the validations are provided by the comparison of the distorted ISAR images between Figure 8(c) (experimental) and Figure 10 (numerical) and between the experimental image and simulated image in Figure 11. These comparisons have clearly demonstrated that the phase modulation effect offers an accurate picture of the distortion in ISAR images.

6. ISAR DISTORTION ACCORDING TO THE QUADRATIC PHASE EFFECT

It would be helpful and useful to make a comparison of the ISAR distortion as predicted by the phase modulation effect and the quadratic phase effect to see the differences between the two. The quadratic phase distortion assumes a target's rotational motion is constant during the imaging period; that is, $\omega(t) = \omega_0$. Any change in the Doppler frequency during the imaging duration by any of the scatterers on the target is due to a nonlinear Doppler velocity introduced along the radar's line of sight as a result of acceleration from the rotational motion. This can be seen by substituting $\omega(t) = \omega_0$ into (23). The phase factor of the rotating scatterer then becomes

$$\psi(t) = \exp \left[-j \frac{4\pi f_c}{c} \left(x_0 \frac{(\omega_0 t)^2}{2} - y_0 \omega_0 t \right) \right]. \quad (25)$$

Considering a scatterer located at $(0, y_0)$ on a target as shown in Figure 5, (25) then becomes

$$\psi(t) = \exp \left[j \frac{4\pi f_c}{c} y_0 \omega_0 t \right], \quad (26)$$

$\psi(t)$ is a linear function in time; therefore, the instantaneous Doppler frequency $f_D = (2f_c y_0 \omega_0 / c)$ is a constant. In other words, for scatterers that have motions nearly parallel to the x -axis, their Doppler frequency will have very little change and thus there will be very little distortion. For a scatterer

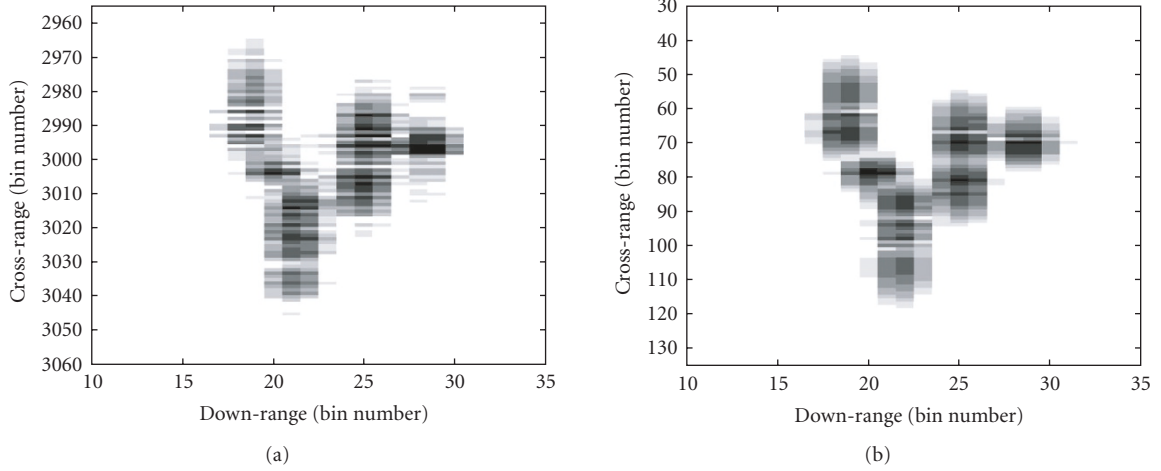


FIGURE 11: Another example of a comparison between (a) experimental distorted ISAR image and (b) computed distorted ISAR image.

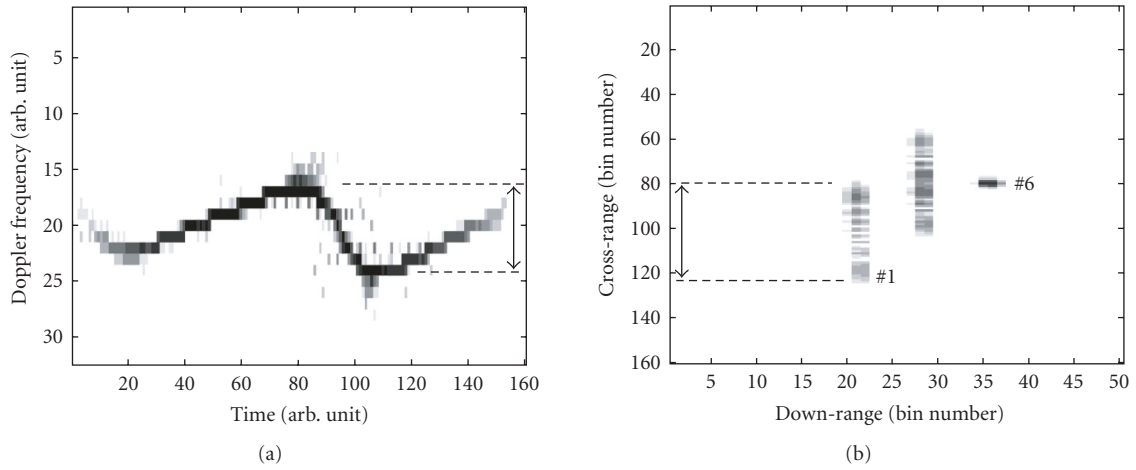


FIGURE 12: (a) Computed Doppler frequency of scatterer #1 on the TMS target during the imaging period, (b) computed ISAR image of scatterer #1 on the TMS target; scatterers #2 and #4 (see Figure 8(d)) are removed in the computation. The amount of distortion of scatterer #1 corresponds to the amount of change in the Doppler frequency.

located at $(x_0, 0)$, (25) becomes

$$\psi(t) = \exp \left[-j \frac{4\pi f_c}{c} x_0 \frac{(\omega_0 t)^2}{2} \right]. \quad (27)$$

Equation (27) displays a phase that is a quadratic function in time. Hence, the Doppler frequency will be changing with time, resulting in a blur in the ISAR image.

To see how much a distorting effect the quadratic phase would have on the ISAR image, a constant ω_0 value corresponding to the maximum value of the experimental rotational rate, $|\omega_{\max}| = 3.9$ degrees/s (as given by the dashed curve in Figure 9(a)), is used in the numerical model for simulating the TMS target. The resulting ISAR image is shown in Figure 15. The amount of distortion in the image is much less than that for the case where a time-varying rotational rate $\omega(t)$ is used. This is quite evident by comparing Figure 15 with Figure 10.

Another interesting observation that is worthy to note is that in the quadratic phase distortion case, the largest distortion occurs at scatterer #6 of the target as seen in Figure 15. The large distortion at scatterer #6 can be explained by the fact that the rate of change of the Doppler frequency is maximum for a scatterer that is moving perpendicular to the radar line of sight (x -axis) as depicted in Figure 5. At the location $(x_0, 0)$ and using (12), the movement of scatterer #6 along the x -axis is given by

$$x(t) = x_0 \cos(\omega_0 t). \quad (28)$$

Its velocity component parallel to the radar line of sight (i.e., x -axis) is

$$v_x = \frac{dx(t)}{dt} = -x_0 \omega_0 \sin(\omega_0 t). \quad (29)$$

Hence, $v_x = 0$ at the initial position $(x_0, 0)$ at time $t = 0$. In other words, the velocity of scatterer #6 is perpendicular

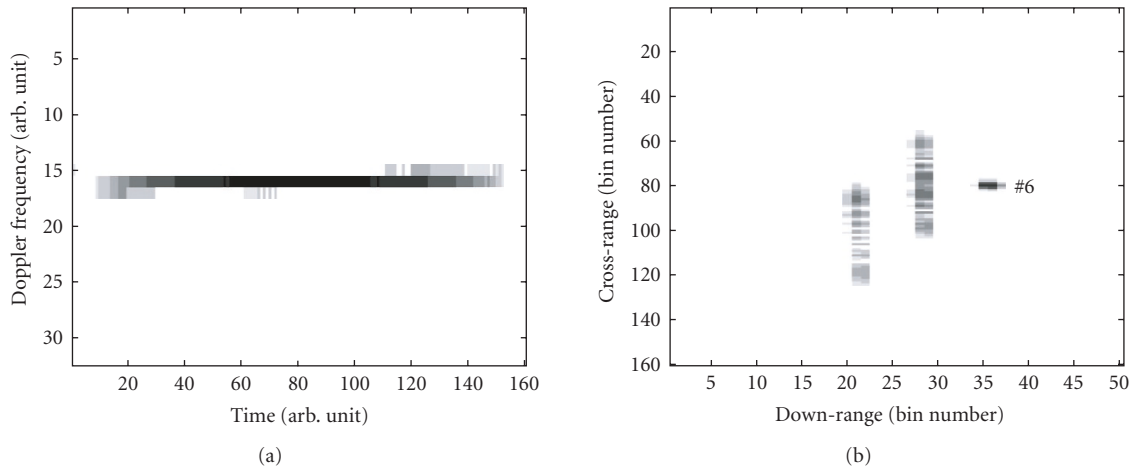


FIGURE 13: (a) Computed Doppler frequency of scatterer #6 of the TMS target during the imaging period, (b) computed ISAR image of the TMS target with scatterers #2 and #4 removed in the computation. The amount of distortion of scatterer #6 corresponds to the amount of change in the Doppler frequency.

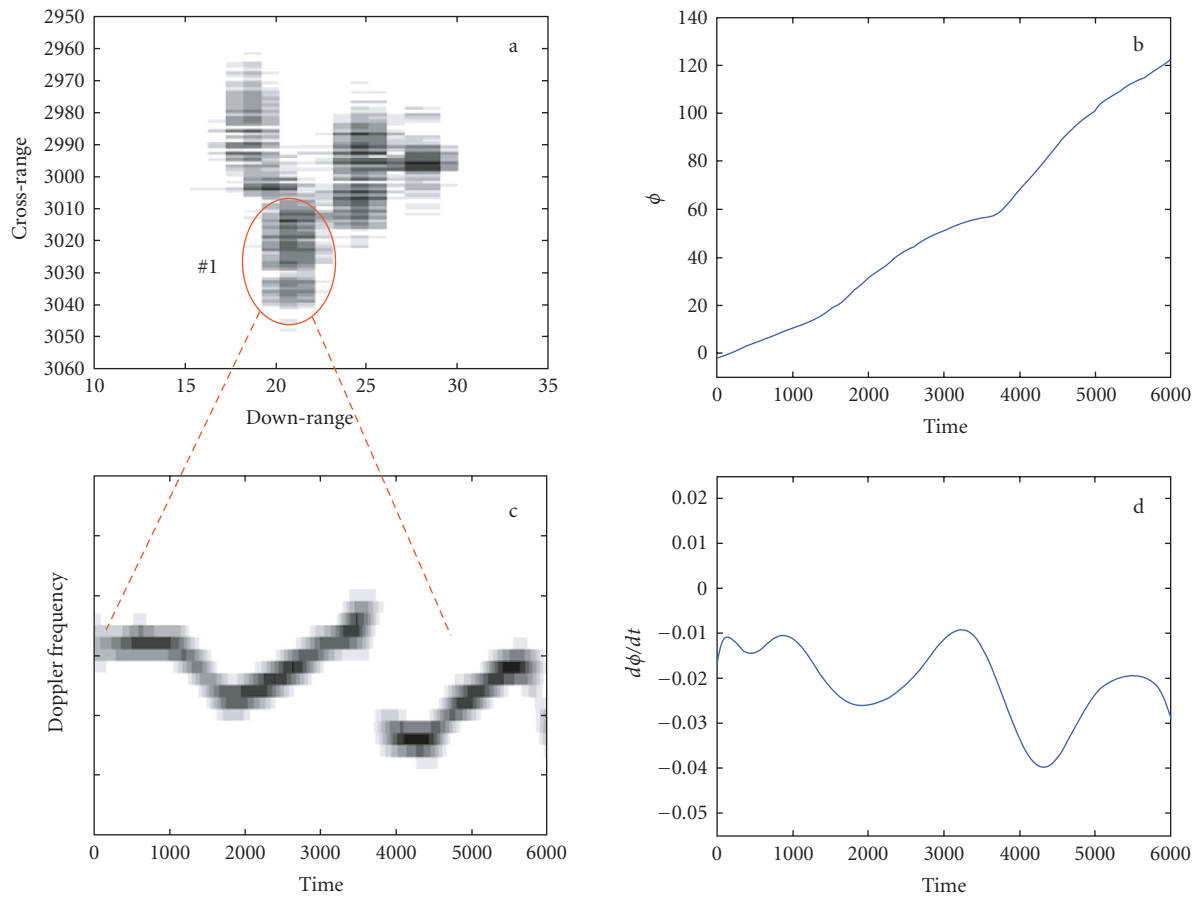


FIGURE 14: A physical interpretation of the phase modulation effect. (a) Distorted ISAR (measured), (b) unwrapped phase (measured), (c) Doppler frequency, and (d) instantaneous frequency of scatterer #1 are shown.

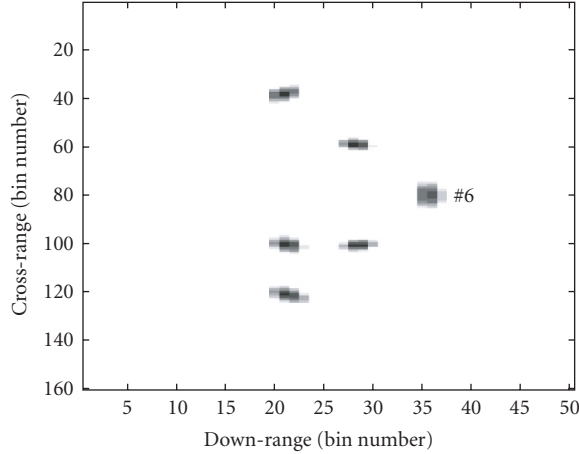


FIGURE 15: Computed ISAR image of the TMS target using a constant rotational rate of 3.9 degrees/s.

to the x -axis; this is intuitively obvious as seen in Figure 5. However, the rate of change of v_x along the radar line of sight

$$\frac{dv_x}{dt} = -x_0\omega_0^2 \cos(\omega_0 t) \quad (30)$$

is maximum at $(x_0, 0)$ because $\cos(\omega_0 t) = 1$ at $t = 0$. This implies that the change in the Doppler frequency will be the largest at scatterer #6; therefore, a notable distortion occurs as a result.

To illustrate the distortion's dependence on $(\omega_0 t)^2$, the ISAR image in Figure 15 is generated using a generously large ω_0 value; that is, $\omega_0 = 3.9$ degrees/s. This corresponds to a target rotation of 15.6 degrees over a 4-second imaging time. In the time-varying rotating case (Figure 10), the target rotation is only 8.2 degrees over the 4-second duration. Using a ω_0 value corresponding to a target rotation of 8 degrees, the quadratic phase case is computed again using a smaller ω_0 value of 2 degrees/s. The resulting ISAR image of the target is shown in Figure 16. It can be seen that none of the scatterers on the target shows any distortion in the image, even scatterer #6 which is expected to display the most distortion. This result is consistent with the experimental ISAR image shown in Figure 8(c), where scatterer #6 displays no noticeable distortion.

As demonstrated in the analysis in this section and in Section 5, it is the temporal variation in the rotation (i.e., $\omega(t)$), not the amplitude of the rotation, that introduces the severe distortion in ISAR images. More precisely, the rate of change in the phase of the target echo $d\phi/dt$, introduced by the time-varying rotation $\omega(t)$, produces a band of instantaneous Doppler frequencies. The distortion in the target's ISAR image is a result of the introduction of this band of Doppler frequencies during the imaging period. In summary, the above analysis shows that the quadratic phase error is not adequate for describing the severe ISAR distortions that are often seen in the experimental images. The quadratic phase error (i.e., $(\omega_0 t)^2$) is a second-order effect and it produces a

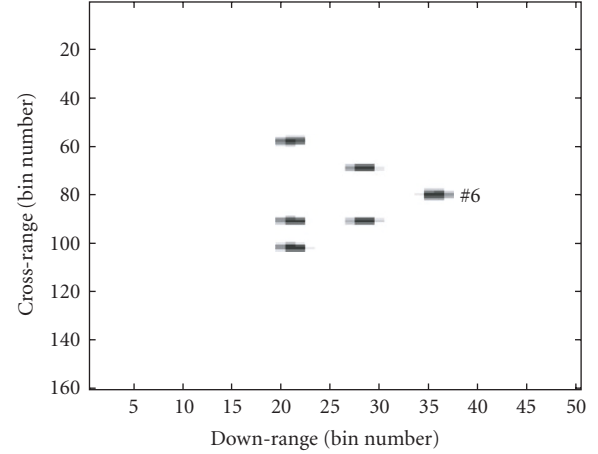


FIGURE 16: Computed ISAR image of the TMS target using a constant rotational rate of 2 degrees/s.

much smaller distortion than that from the phase modulation effect.

7. REFOCUSING OF DISTORTED ISAR IMAGES

According to the principles of ISAR imaging, a long image integration time is required to produce fine image resolution. However, a long image integration time does not always guarantee good cross-range resolution. This is illustrated in the discussion above where it is found that the amount of blurring from integrating the image over the imaging period can be quite severe. As seen from the discussion above, the blurring of ISAR images is a consequence of a time-varying Doppler frequency due to nonuniform motion of the target during the imaging period. Time-frequency techniques have been used successfully to "refocus" blurred ISAR images. By extracting an ISAR image of the target at a particular instant of time, a better-focused image can be obtained because the target's motion can be considered as relatively uniform over a short duration. However, there will be a large number of time instants to deal with in time-frequency processing; thus, a large number of refocused ISAR images will be generated, corresponding to different time instants. For accurate target recognition, it is imperative to make use of only the best refocused image. It is impractical and inefficient to examine all available refocused ISAR images. Visual inspection manually over a large number of images, or even using an automated image search algorithm, only adds extra complexity to the target recognition process.

A more efficient way to determine the optimum refocused ISAR image is possible, based on the insights obtained from the image distortion analysis conducted above. That is to say, it is found from the experimental and numerical analyses that the blurring is directly related to the amount of change in the Doppler frequency of the target during the imaging duration. This fact can be utilized in the refocusing process. The experimental distorted ISAR image in Figure 11(a) will be used as an example to illustrate how a

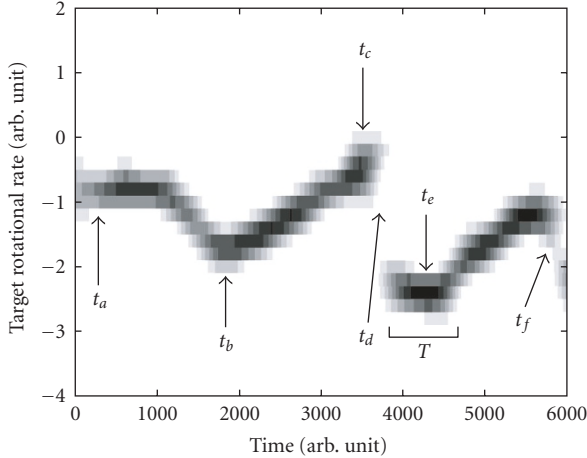


FIGURE 17: The measured temporal motion of the target corresponding to the distorted ISAR image in Figure 11(a). T is the time window width (0.4 second) used in the refocusing process. Six time instants are chosen for the image refocusing.

distorted image can be refocused efficiently. This image is chosen for its varied time-varying target motion over the imaging period; the corresponding rotational motion of the target is shown in Figure 17.

In order to see how an optimum refocused ISAR image can be determined, it is helpful to first take a look at some samples of the refocused images at various time instants. A refocused ISAR image can be reconstructed from the spectrograms at all the down-range bins of the distorted ISAR image at a chosen time instant. The spectrograms are computed using time-frequency methods [11]. In the example discussed here, spectrograms using short-time Fourier transform (STFT) with a 0.4-second image integration time window is employed. In other words, each refocused image is reconstructed from a 0.4-second time segment. Thus it is more accurate to describe a time instant as a short duration of time rather than a precise point in time. Figure 18 shows samples of the refocused ISAR images of the target at the 6 different time instants selected in Figure 17. The ISAR image at time t_a corresponds to the instance when the target has a uniform rotational motion. This image serves as a reference image for comparing with the refocused images at other time instants. Using a 0.4-second STFT, the resolution is just barely adequate to resolve the scatterers on the target in the cross-range direction for the uniform rotation case at t_a . A quick inspection of Figure 18 reveals that the best refocused images are at the time instants t_b and t_c and the worst images are at t_c , t_d , and t_f .

By trying to understand why the worst images are occurring at t_c and t_d , and why the best image is located at t_e , we can develop a methodology for reconstructing the optimum refocused ISAR image quickly. The ISAR image at t_c appears compressed. This is due to a small Doppler frequency (i.e., small angular rotational rate) possessed by the target at this time instant. The Doppler at t_c is even smaller than the

uniform rotation case at t_a ; this is illustrated in Figure 17. This Doppler motion is too small to separate the scatterers adequately in the cross-range direction. The ISAR images at time t_d and t_f still appear blurry, with some of the scatterers still not properly focused. This is due to the fact that the Doppler motion of the target is going through a large temporal rate of change within the time window T ; that is, a large $(f_{D,\max} - f_{D,\min})$ occurs during T . In other words, the target is experiencing a range of Doppler frequencies, causing a smear in the image.

The ISAR image at t_e has all six scatterers on the target clearly resolved and provides the best-refocused image. There are two reasons why the best image quality is found at time instance t_e . Firstly, the Doppler motion is large, significantly larger than the uniform rotational rate case at the time instant t_a (see Figure 17). Hence, the scatterers are separated more along the cross-range dimension by the large angular rotational rate of the target. Secondly, the temporal rate of change of the Doppler motion during the time interval at t_e is small; that is, $(f_{D,\max} - f_{D,\min})/T$ is small. Therefore, the blurring of the image is kept to a minimum. The time window width T at the time instant t_e is indicated in Figure 17. It can be seen that the rotational motion, hence the Doppler frequency, varies very little within the time window.

Based on the analysis of the refocused images shown in Figure 18, we can deduce a few simple physical rules that will enable us to extract a relatively well-focused image from a blurred ISAR image quickly.

- (1) From the blurred image, locate a down-range bin where it contains the most severe blurring in the cross-range. A down-range bin that contains only a single scatterer is desirable, but not necessary.
- (2) Produce a time-frequency spectrogram at the chosen down-range bin, using a time-frequency distribution function [11]. Short-time Fourier transform is used here as an illustration. Distribution functions such as the Wigner-Ville distribution and the Choi-Williams distribution may be used; but for targets with multiple scatterers, cross-term artifacts from these bilinear distribution functions could be an issue.
- (3) From the spectrogram, select a time instant when the variation of the Doppler motion is small (i.e., small $(f_{D,\max} - f_{D,\min})/T$) and the value of the Doppler motion is large (i.e., as far away from the zero Doppler frequency as possible). The time window width T should be large enough to cover a more or less constant Doppler segment.
- (4) Construct spectrograms at all down-range bins from the blurred ISAR image of the target. Recombine all spectrograms at the same time instant to reconstruct a focused ISAR image.

This procedure provides a much faster means of reconstructing a focused image. This is because once the appropriate time instant is determined, only one ISAR image needs to be reconstructed. This is obviously much more efficient than extracting ISAR images at all time instants from all spectrograms because the number of time instants is usually very large.

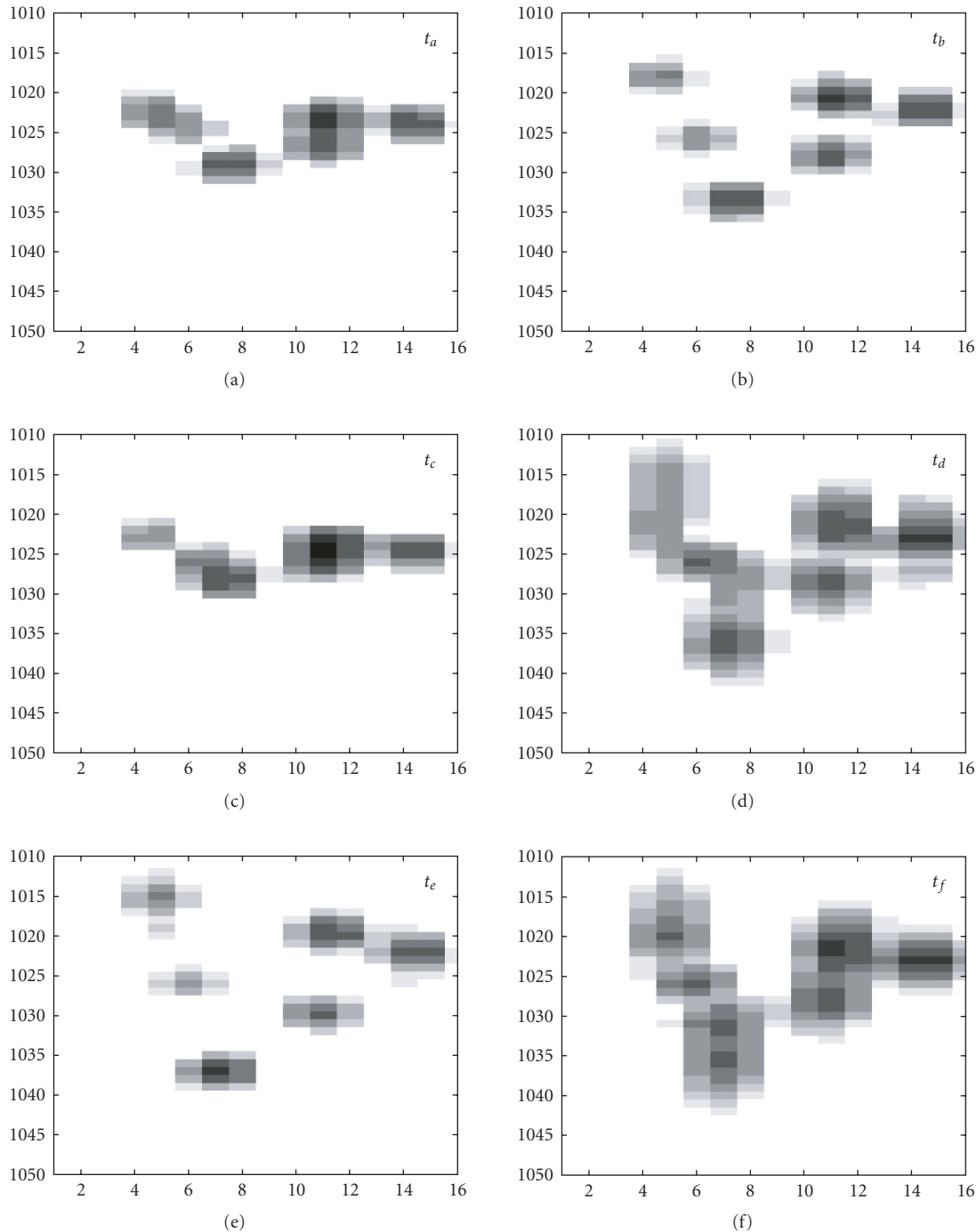


FIGURE 18: Refocused ISAR images of the TMS target from the distorted image in Figure 11(a) at different time instants as indicated in Figure 17.

Although extracting information in a small time interval from the original ISAR image data implies a fundamental loss in cross-range resolution, this loss in resolution can be mitigated, however, by a couple of factors. It is interesting to note that having a large amount of blurring in the ISAR image may actually be better than having just a small amount of blurring for restoring a focused image. A more severe blurring means that at some time instant, there is a large

Doppler motion that can be exploited to get a better cross-range resolution. In addition, the reassignment method in time-frequency processing permits a better-focused image [12]. The reassignment procedure provides an improvement in the localization of the signal energy distribution, thus yielding a sharper image. Refocused ISAR images of real in-flight aircraft using the procedure described in this section are found to have reasonably good quality [13].

8. CONCLUSIONS

From the results of the numerical analysis and the comparisons with experimental data, it is found that the severe distortion in ISAR images can be modelled accurately by including the temporal variation of the target's motion in its angular rotational rate. That is to say, the angular rotation is described as a function of time (i.e., $\omega(t)$) so that an instantaneous Doppler motion can be ascribed at any given time. A band of instantaneous Doppler frequencies introduced during the imaging duration produces a smear in the target's image along the cross-range direction. The distortion mechanism can be viewed as a phase modulation effect in the phase of the target echo. The conventional quadratic phase distortion is a result of nonlinear Doppler motion from a target with a constant circular motion and it may be considered as a special case of the phase modulation effect. The quadratic phase error is not adequate to account for the severe distortion observed in ISAR images. The phase modulation effect is more accurate in quantifying the amount of distortion in ISAR images.

An efficient procedure to find the best-refocused image from a severely blurred image based on time-frequency analysis has also been developed. By applying time-frequency analysis on the distorted target image, one can quickly determine the appropriate time instant and the optimum time window width. This information can be used to quickly refocus the distorted image.

ACKNOWLEDGMENTS

The authors would like to thank V. C. Chen of the Naval Research Laboratory, Washington, for his time and effort in providing comments and inputs to the writing of this manuscript. We would also like to acknowledge the financial support of William Miceli, Office of Naval Research—International Field Office, London, UK, through the NICOP project “Time-Frequency Processing for ISAR Imaging and Non-Cooperative Target Identification” in which the work presented in this manuscript was conducted.

REFERENCES

- [1] T. Sparr, S.-E. Hamran, and E. Korsbakken, “Estimation and correction of complex target motion effects in inverse synthetic aperture imaging of aircraft,” in *Proceedings of IEEE International Radar Conference (RADAR '00)*, pp. 457–462, Alexandria, Va, USA, May 2000.
- [2] V. C. Chen and W. J. Miceli, “Simulation of ISAR imaging of moving targets,” *IEE Proceedings - Radar, Sonar and Navigation*, vol. 148, no. 3, pp. 160–166, 2001.
- [3] Y. Wang, H. Ling, and V. C. Chen, “ISAR motion compensation via adaptive joint time-frequency technique,” *IEEE Transactions on Aerospace and Electronic Systems*, vol. 34, no. 2, pp. 670–677, 1998.
- [4] D. R. Wehner, *High-Resolution Radar*, Artech House, Boston, Mass, USA, 2nd edition, 1995.
- [5] V. C. Chen and W. J. Miceli, “Time-varying spectral analysis for radar imaging of manoeuvring targets,” *IEE Proceedings - Radar, Sonar and Navigation*, vol. 145, no. 5, pp. 262–268, 1998.

- [6] V. C. Chen and H. Ling, *Time-Frequency Transform for Radar Imagery and Signal Analysis*, Artech House, Boston, Mass, USA, 2002.
- [7] A. W. Rihaczek and S. J. Hershkowitz, “Identification of targets from ISAR images,” in *NATO Symposium on Target Identification and Recognition Using RF Systems*, Oslo, Norway, October 2004.
- [8] T. Sparr and B. Krane, “When are time-frequency methods useful for radar signature analysis,” in *NATO Symposium on Target Identification and Recognition Using RF Systems*, Oslo, Norway, October 2004.
- [9] S. K. Wong, G. Duff, and E. Riseborough, “Distortion in the inverse synthetic aperture radar (ISAR) images of a target with time-varying perturbed motion,” *IEE Proceedings - Radar, Sonar and Navigation*, vol. 150, no. 4, pp. 221–227, 2003.
- [10] S. K. Wong, G. Duff, and E. Riseborough, “Analysis of distortion in the high range resolution profile from aperturbed target,” *IEE Proceedings - Radar, Sonar and Navigation*, vol. 148, no. 6, pp. 353–362, 2001.
- [11] L. Cohen, “Time-frequency distributions—a review,” *Proceedings of the IEEE*, vol. 77, no. 7, pp. 941–980, 1989.
- [12] F. Auger, P. Flandrin, P. Goncalves, and O. Lemoine, “Time-Frequency Toolbox for Use in MATLAB,” Tutorial, July 15, 1997, <http://www.nongnu.org/tftb/>.
- [13] S. K. Wong, E. Riseborough, and G. Duff, “Application of phase modulation to ISAR image processing and countermeasures against radar imaging,” in *Combat Identification Systems Conference*, Portsmouth, Va, USA, May 2005, Session 5, Paper 6.

S. K. Wong received his B.S. degree in physics from the University of British Columbia, Canada, in 1978, his M.A.S. and Ph.D. degrees in aerospace science from the University of Toronto in 1980 and 1985, respectively. He joined the Defence Research Establishment Valcartier, Canada, in 1986. From 1986 to 1995, he worked on solid-state lasers and nonlinear optics. He moved to the Defence Research Establishment Ottawa in 1995 where he worked on noncooperative target recognition, synthetic radar target signature generation, and inverse synthetic aperture radar imaging. Currently, he is working on multistatic SAR/ISAR imaging.



E. Riseborough received the B.Eng. degree in electrical engineering from Carleton University, Ottawa. In 1981, he joined IP Sharp Associates where he worked as a Systems Engineer. In 1987, he joined AIT Corporation where he worked on the development of an experimental array radar system for studying the tracking of low-elevation targets in the presence of multipath. He joined the Defence Research Establishment Ottawa in 1990 where he continued the low angle tracking research, modified the experimental radar to study jammer suppression for multifunction radar, and studied high range resolution and inverse synthetic aperture radar. His present work is in detection and tracking of low observable targets in sea clutter at DRDC Ottawa where he leads the Radar Technology Group.



G. Duff attended the University of Alberta in Electrical Engineering in 1954 and graduated from the Southern Alberta Institute of Technology in 1957. He has been employed as a technologist with several Canadian government research agencies since the early fifties starting with the Department of Agriculture and subsequently the Defense Research Board, the Communications Research Center, the Defense Research Establishment Ottawa, and lately with the Defense Research and Development Canada Corporation. His technical expertise is in the areas of electronics, interfacing radar hardware with computer equipment, design of experimental apparatus and data acquisition systems. He has worked in the fields of computer and radar technology area for over 50 years.

